Title
Effective Optical Properties of Absorbing Nanoporous and Nanocomposite Thin-Films

Journal
Journal of Applied Physics, 101

Authors
Garahan, Anna
Pilon, Laurent
Yin, Juan
et al.

Publication Date
2007-01-14

DOI
10.1063/1.2402327

Peer reviewed

Effective Optical Properties of Absorbing Nanoporous and Nanocomposite Thin Films

Anna Garahan, Laurent Pilon, Juan Yin,
Mechanical and Aerospace Engineering Department
Henry Samueli School of Engineering and Applied Science
University of California, Los Angeles - Los Angeles, CA 90095, USA
Phone: +1 (310)-206-5598, Fax: +1 (310)-206-4830
E-mail: pilon@seas.ucla.edu

and

Indu Saxena
Intelligent Optical Systems, Inc., Torrance, CA 90505

January 25, 2007

Abstract

This paper aims at developing numerically validated models for predicting the through-plane effective index of refraction and absorption index of nanocomposite thin films. First, models for the effective optical properties of such materials are derived from previously reported analysis applying the volume averaging theory (VAT) to the Maxwell's equations. The transmittance and reflectance of nanoporous thin films are computed by solving the Maxwell's equations and the associated boundary conditions at all interfaces using finite element methods. The effective optical properties of the films are retrieved by minimizing the root mean square of the relative errors between the computed and theoretical transmittance and reflectance. Nanoporous thin films made of SiO_2 and TiO_2 consisting of cylindrical nanopores and nanowires are investigated for different diameters and various porosities. Similarly, electromagnetic wave transport through dielectric medium with embedded metallic nanowires are simulated. The numerical results are compared with predictions from widely used effective property models including (1) the Maxwell-Garnett Theory, (2) the Bruggeman effective medium approximation, (3) the parallel, (4) series, (5) Lorentz-Lorenz, and (6) the VAT models. Very good agreement is found with the VAT model for both the effective index of refraction and absorption index. Finally, the effect of volume fraction on the effective index of refraction and absorption index predicted by the VAT model is discussed. For certain values of wavelengths and volume fractions, the effective index of refraction or absorption index of the composite material can be smaller than that of both the continuous and dispersed phases. These results indicate guidelines for designing nanocomposite materials with desired optical properties.

1 Introduction

In recent years, synthesis and characterization of nanocomposite thin films in general and nanoporous in particular, have been the subject of intense study [1, 2, 3, 4]. Potential applications include dye-sensitized solar cells [5, 6, 7], low-k dielectric materials [8, 9], biosensors [10, 11, 12], and optical devices including waveguides [13, 14, 15], Bragg reflectors and Fabry-Perot filters [16, 17, 18, 19, 20, 21, 22]. For example, in order to confine and propagate electromagnetic waves within a waveguide, the guide region itself must have a higher index of refraction than the surrounding cladding [23]. On the other hand, Bragg reflectors and Fabry-Perot filters are built by generating alternating layers with prescribed thickness and index of refraction. This geometry uses constructive and destructive interferences to selectively reflect or transmit at desired wavelengths. In each of these optical applications, the index of refraction is tuned by controlling the morphology and porosity of the nanosize pores formed by electrochemical etching of silicon, for example. Optimizing the performance of a given component requires accurate knowledge of the effect of porosity, pore shape and size as well as the optical properties of each phase on the effective optical properties of the nanocomposite medium.

Various effective property models have been proposed in the literature and were discussed in our previous study [24]. In brief, the Maxwell-Garnett Theory (MGT) [25] was first developed to model the effective electric permittivity of heterogeneous media consisting of monodispersed spheres arranged in a cubic lattice structure within a continuous matrix and of diameter much smaller than the wavelength of the incident electromagnetic (EM) wave. Then, the effective dielectric constant $\epsilon_{r,eff}$ is expressed as,

$$\epsilon_{r,eff} = \epsilon_{r,c}\left[1 - \frac{3\phi(\epsilon_{r,c} - \epsilon_{r,d})}{2\epsilon_{r,c} + \epsilon_{r,d} + \phi(\epsilon_{r,c} - \epsilon_{r,d})}\right] \tag{1}$$

where $\epsilon_{r,c}$ and $\epsilon_{r,d}$ are the dielectric constant of the continuous and dispersed phases, respectively, while ϕ is the porosity. For dispersed phase volume fractions larger than $\pi/6 \simeq 52\%$ and polydispersed spheres the Bruggeman [26] model gives the following implicit equation

for $\epsilon_{r,eff}$,

$$1-\phi = \frac{\left(\frac{\epsilon_{r,eff}}{\epsilon_{r,c}} - \frac{\epsilon_{r,d}}{\epsilon_{r,c}}\right)}{\left[\left(\frac{\epsilon_{r,eff}}{\epsilon_{r,c}}\right)^{1/3}\left(1-\frac{\epsilon_{r,d}}{\epsilon_{r,c}}\right)\right]} \tag{2}$$

On the other hand, the Lorentz-Lorenz model gives the effective index of refraction n_{eff} as,

$$\left(\frac{n_{eff}^2-1}{n_{eff}^2+2}\right) = (1-\phi)\left(\frac{n_c^2-1}{n_c^2+2}\right) + \left(\phi\frac{n_d^2-1}{n_d^2+2}\right) \tag{3}$$

where n_c and n_d are the index of refraction of the continuous and dispersed phases, respectively. Alternatively, the parallel model gives the effective property ψ_{eff} as a linear function of the properties of the continuous and dispersed phases, i.e.,

$$\psi_{eff} = (1-\phi)\psi_c + \phi\psi_d \tag{4}$$

The series model, on the other hand, is expressed as,

$$\frac{1}{\psi_{eff}} = \frac{1-\phi}{\psi_c} + \frac{\phi}{\psi_d} \tag{5}$$

In addition, del Rio *et al.* [27] suggested the following effective model for electrical conductivity based on the reciprocity theorem,

$$\sigma_{eff} = \sigma_c \frac{1+\phi\left(\sqrt{\sigma_c/\sigma_d}-1\right)}{1+\phi\left(\sqrt{\sigma_d/\sigma_c}-1\right)} \tag{6}$$

Recently, del Rio and Whitaker [28, 29] applied the volume averaging theory (VAT) to the Maxwell's equations for an ensemble of dispersed domains of arbitrary shape in a continuous matrix. They predicted the effective dielectric constant $\epsilon_{r,eff}$, relative permeability $\mu_{r,eff}$, and electrical conductivity σ_{eff} of a two-phase mixture as [28],

$$\epsilon_{r,eff} = (1-\phi)\epsilon_{r,c} + \phi\epsilon_{r,d} \tag{7}$$

$$1/\mu_{r,eff} = (1-\phi)/\mu_{r,c} + \phi/\mu_{r,d} \tag{8}$$

$$\sigma_{eff} = (1-\phi)\sigma_c + \phi\sigma_d \tag{9}$$

The range of validity of these expressions was discussed in details, and a set of inequalities to be satisfied was developed by Del Rio and Whitaker [28]. Their model has been numerically validated by Braun and Pilon [24] for the effective through-plane index of refraction

of *non-absorbing* nanoporous media with open and closed cylindrical nanopores of various shapes and sizes corresponding to a wide range of porosity. The other models however, underpredicted the numerical results [24].

Moreover, validation of the above models against experimental data often yields contradictory results [30]. These contradictions can be attributed to the fact that first, some of these models were not developed for the index of refraction but for the dielectric constant. However, they have been used for optical properties (e.g., Ref.[8, 9, 31, 13]). Second, unlike the present study, some of these models have also been derived by considering a unit cell containing one pore with uniform incident electromagnetic fields thus ignoring possible interference taking place between adjacent pores [25, 26, 32]. Finally, large experimental uncertainty may exist in the measure of the porosity and the retrieval of the complex index of refraction from transmittance and reflectance measurements. The latter is very sensitive to the surface roughness of the film and to the uniformity and value of the film thickness. Unfortunately, often, neither the film thickness L nor the experimental uncertainty for both ϕ and m_{eff} are reported.

The present study extends our previous investigation to *absorbing* nanocomposite thin films. It aims at modeling both the through-plane effective index of refraction and absorption index of (1) nanoporous thin films consisting of horizontally aligned cylindrical nanopores or nanowires with different diameters and various porosities and of (2) dielectric medium with embedded metallic nanowires. Such thin films are anisotropic and this study focuses on properties in the direction normal to the film surface. It is limited to non-magnetic materials for which $\mu_{r,c} = \mu_{r,d} = \mu_{r,eff} = 1$. Spectral normal-normal transmittance and reflectance are obtained by numerically solving the Maxwell's Equations and used to retrieve the effective index of refraction and absorption index. The numerical results are then compared with previously reviewed models. Finally, the VAT model is analyzed in details.

2 Analysis

2.1 Optical Properties From Volume Averaging Theory

The index of refraction n and the absorption index k of homogeneous media can be expressed in terms of the real part of their dielectric constant ϵ_r and of their electrical conductivity σ as [23],

$$n^2 = \frac{1}{2}\left[\epsilon_r + \sqrt{\epsilon_r^2 + \left(\frac{\lambda\sigma}{2\pi c_0 \epsilon_0}\right)^2}\right] \tag{10}$$

$$k^2 = \frac{1}{2}\left[-\epsilon_r + \sqrt{\epsilon_r^2 + \left(\frac{\lambda\sigma}{2\pi c_0 \epsilon_0}\right)^2}\right] \tag{11}$$

where λ is the wavelength of incident radiation, c_0 is the speed of light in vacuum, and ϵ_0 is the permittivity of free space. The expression derived by Del Rio and Whitaker [28] for the effective dielectric constant $\epsilon_{r,eff}$ and electrical conductivity σ_{eff} of a two-phase medium [Equations (7) and (9)] can be used to derive the effective optical properties of a two-phase nanocomposite material,

$$n_{eff}^2 = \frac{1}{2}\left[A + \sqrt{A^2 + B^2}\right] \tag{12}$$

$$k_{eff}^2 = \frac{1}{2}\left[-A + \sqrt{A^2 + B^2}\right] \tag{13}$$

where

$$A = \epsilon_{r,eff} = \phi(n_d^2 - k_d^2) + (1-\phi)(n_c^2 - k_c^2) \tag{14}$$

$$\text{and} \qquad B = \frac{\lambda\sigma_{eff}}{2\pi c_0 \epsilon_0} = 2n_d k_d \phi + 2n_c k_c (1-\phi) \tag{15}$$

In particular, when the dispersed phase is vacuum, $\epsilon_{r,d} = n_d = 1$, and $k_d = \sigma_d = 0$. Note also that, unlike other effective property models, the above VAT models for n_{eff} and k_{eff} depend on both the real and complex parts of the complex indices of refraction of the dispersed and continuous phases. In other words, k_c and k_d affect not only k_{eff} but also n_{eff}.

2.2 Governing Equations and Numerical Implementation

In order to develop the numerical model, let us first consider a surrounding environment (medium 1, n_1, $k_1 = 0$) from which an electromagnetic wave is incident on an absorbing thin

film (medium 2, n_2, k_2) deposited onto an absorbing dense substrate (medium 3, n_3, k_3). A linearly polarized plane wave in transverse electric (TE) mode is incident normal to the film top surface and propagates through the two-dimensional thin film along the x-direction. As the wave propagates in the x-y plane, it has only one electric field component in the z-direction, while the magnetic field has two components in the x-y plane (i.e., perpendicularly polarized), such that in a general time-harmonic form,

$$\vec{E}(x,y,t) = E_z(x,y)e^{i\omega t}\vec{e}_z \qquad \text{and} \qquad \vec{H}(x,y,t) = [H_x(x,y)\vec{e}_x + H_y(x,y)\vec{e}_y]e^{i\omega t} \tag{16}$$

Here, $\vec{E}$ is the electric field vector, $\vec{H}$ is the magnetic field vector, $\vec{e}_x$, $\vec{e}_y$, and $\vec{e}_z$ are the unit vectors, and $\omega = 2\pi c_0/\lambda$ is the angular frequency of the wave. For general time-varying fields in a conducting medium, the Maxwell's Equations can be written as,

$$\nabla \times \left[\frac{1}{\mu_r\mu_0}\nabla \times \vec{E}(x,y,t)\right] - \omega^2\epsilon_r^*\epsilon_0\vec{E}(x,y,t) = 0 \tag{17}$$

$$\nabla \times \left[\frac{1}{\epsilon_r^*\epsilon_0}\nabla \times \vec{H}(x,y,t)\right] - \omega^2\mu_r\mu_0\vec{H}(x,y,t) = 0 \tag{18}$$

where μ_0 and μ_r are the magnetic permeability of vacuum and the relative magnetic permeability, respectively, while ϵ_r^* $(= n^2 - k^2 - i2nk)$ is the complex dielectric constant. The associated boundary conditions are,

$$\vec{n} \times (\vec{H}_1 - \vec{H}_2) = 0 \qquad \text{at the surroundings-film interface} \tag{19}$$

$$\vec{n} \times \vec{H} = 0 \qquad \text{at symmetry boundaries} \tag{20}$$

$$\sqrt{\mu_r\mu_0}(\vec{n} \times \vec{H}) + \sqrt{\epsilon_0\epsilon_r^*}\vec{E} = 0 \qquad \text{at the film-substrate interface} \tag{21}$$

$$\sqrt{\mu_0\mu_r}(\vec{n} \times \vec{H}) + \sqrt{\epsilon_0\epsilon_r^*}\vec{E} = 2\sqrt{\epsilon_0\epsilon_r^*}\vec{E}_0 \qquad \text{at the source surface} \tag{22}$$

where $\vec{n}$ is the normal vector to the appropriate interface. Equation (21) corresponds to the impedance boundary condition for a semi-infinite substrate while Equation (22) is the low reflecting boundary condition to model the imaginary source surface where the incident electromagnetic wave $\vec{E}_0 = E_0\vec{e}_z$ is emitted and that is transparent to the reflected waves.

Moreover, the Poynting vector $\vec{\pi}$ is defined as the cross product of the electric and magnetic vectors, $\vec{\pi} = \frac{1}{2}Re\{\vec{E} \times \vec{H}\}$. Its magnitude corresponds to the energy flux carried by

the propagating electromagnetic wave. Averaging the x-component of the Poynting vector at location (x,y) over a period $2\pi/\omega$ of the EM wave gives [23],

$$|\pi_x|_{avg}(x,y) = -\frac{1}{2}Re\{E_z H_y^*\} \qquad \text{and} \qquad |\pi_y|_{avg}(x,y) = \frac{1}{2}Re\{E_z H_x^*\} \tag{23}$$

The incident electric field $\vec{E}_0 = E_{0z}\vec{e}_z$ and therefore, the incident time-averaged Poynting vector $|\vec{\pi}_0|_{avg}$ are imposed at all locations along the source surface. The values of the the x-component of the Poynting vector along the film-substrate interface are then calculated numerically and averaged along the boundary to yield $|\pi_{x,t}|_{avg}$. The transmittance of the thin film is then recovered by taking the ratio of the transmitted to the incident average Poynting vectors, i.e., $T_{num} = |\pi_{x,t}|_{avg}/|\pi_{x,0}|_{avg}$. Similarly, the magnitude of the x-component of the reflected time-averaged Poynting vector $|\pi_{x,r}|_{avg}$ is computed numerically, and the reflectance of the film is computed according to $R_{num} = |\pi_{x,r}|_{avg}/|\pi_{x,0}|_{avg}$.

Finally, the above equations were solved numerically using a commercially available finite element solver (FEMLAB 3.0) applying the Galerkin finite element method on unstructured meshes. The two-dimensional Maxwell's equations are solved in the frequency domain using a 2D transverse electric (TE) wave formulation as described by Equation (16). In particular, the discretization uses second order elements to solve for the electric field [33].

In order to validate the numerical implementation of this system of equations, a system composed of a dense absorbing thin film ($n_2 = 1.7$, k_2) of thickness L deposited on a perfectly reflective substrate ($n_3 = k_3 \rightarrow \infty$) in air ($n_1$=1, k_1=0) was simulated. The value of k_2 was varied over 3 orders of magnitude from 0.001 to 1, and the infinitely large optical constants of the substrate were imposed as $n_3 = k_3 = 10^6$. Normal reflectivity of the system was computed and plotted as a function of $\pi L/\lambda$ [30]. The numerical solutions match the analytical solutions found in Ref.[23], for example.

Figure 1 schematically shows the geometry of the simulated nanocomposite thin film on a semi-infinite substrate. The Maxwell's equations are solved in both phases separately as previously described. Equation (19) is used as the boundary condition not only at the incident vacuum-film interface but also at all continuous/dispersed phase interfaces. Figure 1 is a schematic representation of an actual model consisting of three nanopores or nanowires

of diameter D=10 nm and cell width H of 20 nm corresponding to a volume fraction $\phi = \pi D^2/4H^2$ =0.1963. Figure 1 also indicates material properties of the different domains and the locations at which each of the boundary conditions are applied. Note that the lines separating two adjacent cubic cells do not correspond to an actual boundary conditions.

Finally, it is important to note that Maxwell's equations are generally applied to macroscopic averages of the fields which can vary widely in the vicinity of individual atoms where they undergo quantum mechanical effects. In addition, both the matrix and the nanodomains are treated as homogeneous and isotropic with index of refraction n and absorption index k equal to that of the bulk.

2.3 Retrieval of Effective Complex Index of Refraction

The effective complex index of refraction of the nanocomposite thin film was retrieved by minimizing the root mean square of the relative error for the transmittance δT and reflectance δR defined as,

$$\delta T^2 = \frac{1}{N}\sum_{i=1}^{N}\left[\frac{T_{calc}(\lambda_i) - T_{num}(\lambda_i)}{T_{num}(\lambda_i)}\right]^2 \quad \text{and} \quad \delta R^2 = \frac{1}{N}\sum_{i=1}^{N}\left[\frac{R_{calc}(\lambda_i) - R_{num}(\lambda_i)}{R_{num}(\lambda_i)}\right]^2 \tag{24}$$

where $T_{num}(\lambda_i)$ and $R_{num}(\lambda_i)$ are the transmittance and reflectance computed numerically using FEMLAB 3.0 while $T_{calc}(\lambda_i)$ and $R_{calc}(\lambda_i)$ are the transmittance and reflectance predicted from electromagnetic wave theory at N different wavelengths λ_i between 400 and 900 nm.

In predicting the theoretical transmittance T_{calc} and reflectance R_{calc} from EM wave theory, polarization effects are disregarded since (1) the incident EM wave is normal to the surface, i.e., the plane of incidence is not defined and the components of the polarization cannot be distinguished [23] and (2) scattering is neglected as the nanopores or nanowires are much smaller than the wavelength of the EM wave. In addition, non-linear optical effects are neglected and surface waves are not observed in the current situation as resonance modes were not excited for the materials and wavelengths considered. Finally, we assume that all interfaces are optically smooth, i.e., surface roughness is much smaller than the wavelength

of the incident EM wave. This assumption may not be satisfied in practice and scattering by the sometimes rough film surface can be observed [34, 35, 36].

The Microsoft Excel Solver based on the generalized reduced gradient nonlinear optimization method [37] was used to identify the optimum n_{eff} and k_{eff} that minimizes the root mean square δT and δR. The theoretical transmittance and reflectance for homogeneous thin films under normal incidence are expressed as [38],

$$T_{calc}(\lambda) = \frac{\tau_{12}\tau_{23}e^{-\kappa_2 L}}{1+2r_{12}r_{23}e^{-\kappa_2 L}cos(\delta_{12}+\delta_{23}-\zeta_2)+r_{12}^2r_{23}^2e^{-2\kappa_2 L}} \quad (25)$$

$$R_{calc}(\lambda) = \frac{r_{12}^2+2r_{12}r_{23}e^{-\kappa_2 L}cos(\delta_{12}+\delta_{23}-\zeta_2)+r_{23}^2e^{-2\kappa_2 L}}{1+2r_{12}r_{23}e^{-\kappa_2 L}cos(\delta_{12}+\delta_{23}-\zeta_2)+r_{12}^2r_{23}^2e^{-2\kappa_2 L}} \quad (26)$$

where

$$r_{ij}^2 = \frac{(n_i-n_j)^2+(k_i-k_j)^2}{(n_i+n_j)^2+(k_i+k_j)^2}, \quad \tau_{ij}=\frac{n_i}{n_j}\frac{4(n_i^2+k_i^2)}{(n_i+n_j)^2+(k_i+k_j)^2}$$

$$tan\delta_{ij} = \frac{2(n_ik_j-n_jk_i)}{n_i^2+k_i^2-(n_j^2+k_j^2)}, \quad \kappa_2=4\pi k_2/\lambda, \text{ and } \zeta_2=4\pi n_2/\lambda \quad (27)$$

Here, the subscripts 1 and 3 refer to the the media above and below the nanocomposite thin film treated as an effective homogeneous and referred to by subscript 2. Validation of the retrieval method combined with the numerically computed transmittance was performed by simulating a dense silicon absorbing thin film of thickness L=1 μm surrounded on both sides by vacuum ($n_1 = n_3$ =1.0, $k_1 = k_3$ =0.0) and having a constant complex index of refraction $m_2 = n_2 - ik_2$= 3.5-i0.01 over the spectral interval from 440 to 1700 nm. The values of n_2 and k_2 retrieved with the above mentioned optimization method fall within 9.0×10^{-6} % and 0.06% of the input values, respectively. Therefore, both the numerical simulation tool and the inverse method to retrieve the effective complex index of refraction of nanocomposite thin films from transmittance and reflectance calculations have been validated and can now be used.

3 Results and Discussion

3.1 Absorbing Nanoporous Media

Simulations of electromagnetic wave transport in nanoporous absorbing SiO_2 thin film were conducted for various porosities, film thicknesses, and pore shapes and sizes. First, the continuous phase was assumed to be characterized by constant optical properties n_c=1.44 and k_c=0.01 over the spectral range from 400 to 900 nm while $n_d = n_1 = 1.0$, $k_d = k_1 = k_3 = 0.0$, and $n_3 = 3.39$. The optimization method previously described was used to retrieve the through-plane effective index of refraction n_{eff} and absorption index k_{eff} from the numerically computed transmittance. A numerically converged solution was obtained with more than 50,000 triangular meshes for 250 wavelengths with a 2 nm increment. The pore diameter was 10 or 100 nm while the ratio of the film thickness L to pore diameter D varied from 10 to 200. Finally, for a given pore diameter, the porosity ϕ varied from 0.0 to 0.7 by changing the dimensions of the cubic cells.

Figure 2 shows the evolution of the through-plane effective index of refraction n_{eff} and absorption index k_{eff} as functions of the ratio L/D for a porosity ϕ equal to 0.1963. The thick solid line corresponds to the predictions of the VAT models given by Equations (12) and (13). The data points represent the values retrieved from the numerically computed transmittance by minimizing δT. As established for non-absorbing thin films [24], the effective index of refraction n_{eff} as well as the effective absorption index k_{eff} become independent of both the film thickness and the pore diameter for thick enough films corresponding to $L/D >$ 100 in the cases investigated. In addition, for porosity ϕ=0.1963, the VAT model predicts the retrieved values of n_{eff} and k_{eff} for L/D=200 within 0.13% and 0.075%, respectively. Finally, Figure 3 shows the root mean square δT as a function of the ratio L/D. The value of δT remains small and decreases as the film thickness increases due to smoother interference fringes. It also decreases as the bubble diameter decreases thanks to reduction in scattering by the bubbles. For most cases (except for $L/D < 20$ and D=100 nm), the numerical and calculated transmittances T_{num} and T_{calc} plotted for wavelengths between 400 and 900 nm

are undistinguishable. For example, for D=10 nm, L/D=150, and $\phi = 0.3$, the maximum relative error $|T_{num} - T_{calc}|/T_{num}$ is 0.07% while δT is equal to 2.04×10^{-4}. Note also that (i) all numerical results were converged, i.e., independent of the number of meshes and (ii) the root mean square remains relative small. Thus, the large variations in n_{eff} and k_{eff} observed for small values of L/D are attributed to interferences between nanopores whose effect tend to average out once enough pores are considered. Then, beyond a critical film thickness to pore diameter ratio, the medium behaves as homogeneous with some effective properties.

Moreover, Figure 4 compares the predictions of various effective medium approaches applied to the through-plane effective index of refraction n_{eff} and absorption index k_{eff} of nanoporous thin films as a function of porosity for n_c=1.44, k_c=0.01, n_d=1.0, k_d=0.0, D=10 nm, and L/D=150. Note that the series and reciprocity models cannot be computed for k_{eff} because k_d=0.0. As intuitively expected, n_{eff} and k_{eff} decrease as the porosity increases. Overall, good agreement is found between the VAT model and the numerical results while the parallel, series, Maxwell-Garnett, and reciprocity models applied to n_{eff} and k_{eff} underpredict the numerical values. The same conclusions were obtained when considering the effective index of refraction of *non-absorbing* nanoporous thin films [24]. Note that the values of n_{eff} predicted by the Lorentz-Lorenz equation [39] fell within 0.2% of the predictions of the Maxwell-Garnett model and therefore, were omitted in Figure 4 for the sake of clarity. In addition, when the pores are open and consist of a set of alternating columns of dispersed and continuous phase, perpendicular to the substrate, the dielectric constant can be modelled using the parallel model given by Equation (7) [30]. Therefore, the VAT model for both n_{eff} and k_{eff} provides an accurate prediction of the effective optical properties of the nanoporous thin films simulated with various pore sizes and porosities. The other effective property models appear not to be appropriate for the reasons previously discussed.

In addition, spectral calculations for nanoporous TiO_2 over the spectral range from 400 to 900 nm have been performed for cylindrical nanopores and nanowires of diameter D=10

nm and for porosity of 0.2146 as illustrated in Figure 5. The overall film thickness L was such that L/D=150 to ensure that the heterogeneous thin film behaves as homogeneous with some effective properties. The spectral dependency of the complex index of refraction of bulk TiO_2 was accounted for by fitting reported experimental data [40] with a second order polynomial to yield,

$$n_{c,\lambda} = 2.179 - 3.234 \times 10^{-4}\lambda + 7.967 \times 10^{-8}\lambda^2 \quad (28)$$

$$k_{c,\lambda} = 8.501 \times 10^{-4} + 1.264 \times 10^{-5}\lambda - 9.362 \times 10^{-9}\lambda^2 \quad (29)$$

where the wavelength λ is expressed in nanometers and varies between 400 and 900 nm. First, the transmittance and reflectance computed for cylindrical pores embedded in a TiO_2 matrix and for cylindrical TiO_2 nanowires (Figure 5) were found to be identical. This indicates that the beyond a critical film thickness, the pore shape has no effect on the effective optical properties of the nanocomposite materials as found by Braun and Pilon [24] for non-absorbing nanoporous thin films. Note that the top surface of the thin film is optically smooth and the film surface roughness due to the presence of nanowires is not accounted for.

Finally, the theoretical transmittance and reflectance were computed using Equations (25) to (27) for an homogeneous thin film having effective spectral index of refraction and absorption index predicted by the VAT model [Equations (12) to (15)]. Figure 6 shows good agreement between the numerical and theoretical transmittances and reflectances of a nanoporous TiO_2 thin film of porosity 0.2146. The maximum absolute errors in transmittance and reflectance were less than 0.03 % and 0.0065 %, respectively and an average relative error less than 3.0%. This confirms the validity of the VAT model on a spectral basis for the effective complex of refraction of nanoporous media consisting of cylindrical pores in an absorbing matrix or of closely packed nanowires.

3.2 Dielectric Medium with Metallic Nanowires

This section aims at assessing the validity of the VAT model for dielectric materials or fluids containing metallic nanowires. Let us consider a dielectric continuous phase of complex

index of refraction m_c=1.4 - i 0.0 containing gold nanowires and having the same index of refraction as bulk gold at 400 nm, i.e., m_d=1.66 - i 1.96 [23]. Two nanowire diameters D are considered namely 10 and 100 nm and, in all cases, the overall film thickness L is such that L/D=150. Then, the film can be treated as homogeneous and effective properties can be defined.

Figure 7 compares the through-plane effective index of refraction and absorption index of the nanocomposite medium retrieved from both numerical transmittance and reflectance with those predicted by the VAT model for volume fraction of nanowires ϕ ranging from 0.0 to 0.7. Note that the retrieved effective optical properties were obtained by minimizing $\delta T + \delta R$ and were very sensitive to the initial guess particularly for D=100 nm when transmittance was very small. In those cases, the properties were retrieved by minimizing only the root mean square δR. Overall, there exist a relatively good agreement between the retrieved values of n_{eff} and k_{eff} at all nanowire volume fractions and for both D=10 and 100 nm. The VAT model predicts the retrieved effective index of refraction n_{eff} within $\pm$6.2% and the effective absorption index k_{eff} within $\pm$ 2.9 %. The fact that metallic nanowires have size dependent optical properties has been ignored but can be accounted for provided that these properties be measured independently.

Moreover, it is interesting to note that the presence of a strongly absorbing dispersed phase such as metallic nanowires reduces dramatically the effective index of refraction of the composite medium even for small volume fractions ϕ. For certain values of ϕ, the effective index of refraction n_{eff} is smaller than that of either the continuous or dispersed phases, i.e., $n_{eff} \leq Min(n_c, n_d)$. It also reaches a minimum at the volume fraction ϕ_1=0.25 as discussed in details in the next section. Simultaneously, the effective absorption index increases significantly even for small metallic nanowire volume fractions. Note also that if the film is thick enough for the effective medium approximation to be valid, the metallic nanowires can take various shapes and/or sizes without affecting the above predictions.

Finally, scattering by the nanopores and nanoparticles can be neglected if their size is much smaller than the wavelength of the incident radiation [41, 42]. A quantitative

criterion requires that the size parameter $\chi = \pi D/\lambda$ be much smaller than unity [41]. This assumption is typically valid for absorbing nanocomposite materials and nanofluids in the visible and infrared part of the spectrum. In the present study χ varies between 0.011 and 0.25. In estimating T_{calc} and R_{calc} from EM wave theory, the fraction of energy scattered by nanopores or nanowires was neglected compared with that transmitted and reflected by the film along the incident direction. This assumption was confirmed numerically for all reported results by comparing the magnitude of the y-component of the Poynting vector perpendicular to the incident directions with its x-component at all locations in the x-y plane, i.e., $|\pi_y|_{avg} \ll |\pi_x|_{avg}$.

3.3 Discussion of the Effective VAT Model

The objective of this section is to mathematically analyze the now numerically validated expressions of n_{eff} and k_{eff} given by Equations (12) and (13). Their derivatives with respect to volume fraction ϕ are expressed as,

$$\frac{\partial n_{eff}^2}{\partial \phi} = \frac{1}{2}\left[\alpha + (A^2+B^2)^{-\frac{1}{2}}(A\alpha + B\beta)\right] \tag{30}$$

$$\frac{\partial k_{eff}^2}{\partial \phi} = \frac{1}{2}\left[-\alpha + (A^2+B^2)^{-\frac{1}{2}}(A\alpha + B\beta)\right] \tag{31}$$

where

$$\alpha = \frac{\partial A}{\partial \phi} = (n_d^2 - k_d^2) - (n_c^2 - k_c^2) \qquad \text{and} \qquad \beta = \frac{\partial B}{\partial \phi} = 2(n_d k_d - n_c k_c) \tag{32}$$

Note that the derivatives of A and B with respect to porosity ϕ denoted by α and β, respectively, are independent of porosity. The effective properties n_{eff} and k_{eff} reach their maximum or minimum when the first order derivatives with respect to volume fraction vanish, i.e., when

$$\left(A^2+B^2\right)^{-\frac{1}{2}}(A\alpha + B\beta) = -\alpha \tag{33}$$

$$\text{and} \qquad \left(A^2+B^2\right)^{-\frac{1}{2}}(A\alpha + B\beta) = \alpha \tag{34}$$

Squaring both sides of Equations (33) and (34) yields the same second order polynomial in terms of the volume fraction ϕ. Given the complex index of refraction of both phases, one

can solve for the critical volume fraction corresponding to a minimum and/or maximum of the effective index of refraction and/or absorption index. After rearrangement two roots ϕ_1 and ϕ_2 can be found,

$$\phi_1 = \frac{2\left[(\alpha^2-\beta^2)n_c k_c - \alpha\beta(n_c^2-k_c^2)\right]}{\beta(\alpha^2+\beta^2)} \tag{35}$$

$$\phi_2 = \frac{n_c k_c}{n_c k_c - n_d k_d} \tag{36}$$

In order to know whether n_{eff} and k_{eff} reach their maximum or minimum, their second order derivatives with respect to ϕ have to be examined. Based on Equations (33) and (34), the second order derivatives of n_{eff} or k_{eff} are the same for ϕ_1 and ϕ_2 and can be expressed as,

$$\left.\frac{\partial^2 n_{eff}}{\partial\phi^2}\right|_{\phi_{1,2}} = \frac{1}{4n_{eff}}\frac{(A\beta-B\alpha)^2}{(A^2+B^2)^{\frac{3}{2}}} \tag{37}$$

$$\left.\frac{\partial^2 k_{eff}}{\partial\phi^2}\right|_{\phi_{1,2}} = \frac{1}{4k_{eff}}\frac{(A\beta-B\alpha)^2}{(A^2+B^2)^{\frac{3}{2}}} \tag{38}$$

Since the terms on the right-hand side of the above two equations are always positive, n_{eff} and k_{eff} can only reach a minimum.

However, for an arbitrary set of dispersed and continuous phases, the values of ϕ_1 and ϕ_2 do not always fall in the physically acceptable range of porosities between 0 and 1. For positive values of the properties n_c, n_d, k_c, and k_d, one can show that, unlike ϕ_1, the second root ϕ_2 never falls between 0 and 1.

Moreover, the following expressions can be used to identify whether ϕ_1 is the solution of Equation (33) or (34), i.e., whether n_{eff} or k_{eff} reach a minimum at $\phi = \phi_1$,

$$\chi = \frac{n_d k_d - n_c k_c}{n_c k_c(n_d^2-k_d^2) - n_d k_d(n_c^2-k_c^2)} \tag{39}$$

If χ is strictly positive then k_{eff} reaches a minimum while n_{eff} reaches a minimum if χ is strictly negative. Neither n_{eff} nor k_{eff} reach a minimum if $\chi = 0$. In the case of nanoporous media, χ and ϕ_2 are constant and equal to -1 and 1, respectively. Therefore n_{eff} can reach a minimum less than 1.0 at an acceptable ϕ_1. Finally, for the dielectric medium with embedded

metallic nanowires simulated previously, χ is strictly negative and n_{eff} reaches a minimum. This is illustrated in Figure 7 where n_{eff} reaches a minimum of 1.33 at ϕ_1=0.25.

Finally, this study constitutes the first two-dimensional numerical validation for TE polarization of the VAT applied to the three-dimensional Maxwell's equations [28, 29] in two-phase systems with dispersed domains of arbitrary shape. For complete validation, the present study should be extended to both a three-dimensional and transverse magnetic (TM) polarization cases.

4 Conclusions

The VAT models for the effective dielectric and electrical properties of two-phase media [28] have been used to derive the through-plane effective index of refraction n_{eff} and absorption index k_{eff} of nanoporous materials. Moreover, a numerical scheme has been developed and implemented to solve the Maxwell's equations for a normally incident TE electromagnetic wave travelling through (1) nanoporous SiO_2 and TiO_2 consisting of cylindrical pores or nanowires and (2) dielectric medium containing cylindrical nanowires. All interfaces were treated as optically smooth and the dispersed phase volume fraction varied from 0.0 to 0.7. Calculation were performed on a gray or spectral basis between 400 and 900 nm. The effective optical properties for the simulated nanocomposite thin films were retrieved by minimizing the root mean square of the relative errors for the transmittance and reflectance. In all cases, the results for both k_{eff} and n_{eff} are in good agreement with the predictions from the VAT model. Finally, the numerically validated VAT model is discussed and used to predict the behavior of the optical properties of nanocomposite materials. It shows that under certain conditions, the effective index of refraction or absorption index of the composite material can be smaller than that of both the continuous and dispersed phases. The same results and conclusions are expected for spherical pores and nanoparticles. These results can be used to design and optimize nanocomposite materials with tunable optical properties as well to measure the porosity or nanowire volume fraction provided that the film be thick enough to be treated as homogeneous with some effective properties and that all surfaces be optically

smooth.

Acknowledgements

This work was supported by the National Science Foundation through the CAREER Award Program (CTS 0449429) and by Intelligent Optical Systems, Inc., Torrance, CA.

References

[1] C.J. Brinker, Y. Lu, A. Sellinger, and H. Fan, "Evaporation-induced self-assembly: Nanostructures made easy", *Advanced Materials*, vol. 11, no. 7, pp. 579–585, 1999.

[2] H. Fan, H.R. Bentley, K.R. Kathan, P. Clem, Y. Lu, and C.J. Brinker, "Self-assembled aerogel-like low dielectric constant films", *Journal of Non-Crystalline Solids*, vol. 285, pp. 79–83, 2001.

[3] P.C.A. Alberius, K.L. Frindell, R.C. Hayward, E.J. Kramer, G.D. Stucky, and B.F. Chmelka, "General predictive syntheses of cubic, hexagonal, and lamellar silica and titania mesostructured thin films", *Chemistry of Materials*, vol. 14, pp. 3284–3294, 2002.

[4] B.W. Eggiman, M.P. Tate, and H.W. Hillhouse, "Rhombohedral structure of highly ordered and oriented self-assembled nanoporous silica thin film", *Chemistry of Materials*, vol. 18, pp. 723–730, 2006.

[5] B. O'Regan and M. Grätzel, "A low-cost, high-efficiency solar cell based on dye-sensitized colloidal TiO_2 films", *Nature*, vol. 353, pp. 737–740, 1991.

[6] P. Ravirajan, S. A. Haque, D. Poplavskyy, J. R. Durrant, D. D. C. Bradley, and J. Nelson, "Nanoporous TiO_2 solar cells sensitised with a fluorenethiophene copolymer", *Thin Solid Films*, vol. 451-452, pp. 624–629, 2004.

[7] L. Schmidt-Mende and M. Grätzel, "TiO_2 pore-filling and its effect on the efficiency of solid-state dye-sensitized solar cells", *Thin Solid Films*, vol. 500, pp. 296–301, 2006.

[8] M. I. Sanchez, J. L. Hedrick, and T. P. Russell, "Nanofoam porosity by infrared spectroscopy", *Journal of Polymer Science Part B - Polymer Physics*, vol. 33, no. 2, pp. 253–257, 1995.

[9] M. I. Sanchez, J. L. Hedrick, and T. P. Russell, "Nanofoam porosity measured by infrared spectroscopy and refractive index", in *Microporous and Macroporous Mate-*

rials Materials Research Society Symposium Proceedings, Pittsburgh, PA, USA, 1996, Materials Research Society, vol. 431, pp. 475–480.

[10] R.J. Martin-Palma, V. Torres-Costa, M. Arroyo-Hernandez, M. Manso, J. Perez-Rigueiro, and J.M. Martinez-Duart, "Porous silicon multilayer stacks for optical biosensing applications", *Microelectronics Journal*, vol. 35, pp. 45–48, 2004.

[11] M. Arroyo-Hernandez, R.J. Martin-Palma, J. Perez-Rigueiro, J.P Garcia-Ruiz, J.L. Garcia-Fierro, and J.M Martinez-Duart, "Biofunctionalization of surfaces of nanostructured porous silicon", *Materials Science and Engineering*, vol. 23, pp. 697–701, 2003.

[12] S. Chan, Y. Li, L.J. Rothberg, B.L. Miller, and P.M. Fauchet, "Nanoscale silicon microcavities for biosensing", *Materials Science and Engineering*, vol. 15, pp. 277–282, 2001.

[13] A. Loni, L.T. Canham, M.G. Berger, R. Arens-Fischer, H. Munder, H. Luth, H.F. Arrand, and T.M. Benson, "Porous silicon multilayer optical waveguides", *Thin Solid Films*, vol. 276, pp. 143–146, 1996.

[14] H.F. Arrand, T.M. Benson, A. Loni, M.G. Krueger, M. Thoenissen, and H. Lueth, "Self-aligned porous silicon optical waveguides", *Electronics Letters*, vol. 33, no. 20, pp. 1724–1725, 1997.

[15] A. Jain, S. Rogojevic, S. Ponoth, I. Matthew, W.N. Gill, P. Persans, M. Tomozawa, J.L. Plawsky, and E. Simonyi, "Porous silica materials as low-k dielectrics for electronic and optical interconnects", *Thin Solid Films*, vol. 398, pp. 513–522, 2001.

[16] M.G. Berger, M. Thonissen, R. Arens-Fischer, H. Munder, H. Luth, M. Arntzen, and W. Thei, "Investigation and design of optical properties of porosity superlattices", *Thin Solid Films*, vol. 255, pp. 313–316, 1995.

[17] J. Diener, N. Künzner, D. Kovalev, E. Gross, V.Y. Timoshenko, G. Polisski, and F. Koch, "Dichroic Bragg reflectors based on birefringent porous silicon", *Applied Physics Letters*, vol. 78, no. 24, pp. 3887–8889, 2001.

[18] M. Krüger, M. Marso, M.G. Berger, M. Thönissen, S. Billat, R. Loo, W. Reetz, H. Lüth, S. Hilbrich, R. Arens-Fischer, and P. Grosse, "Color-sensitive photodetector based on porous silicon superlattices", *Thin Solid Films*, vol. 297, pp. 241–244, 1997.

[19] S. Zangooie, M. Schubert, C. Trimble, D.W. Thompson, and J.A. Woollam, "Infrared ellipsometry characterization of porous silicon Bragg reflectors", *Applied Optics*, vol. 40, no. 6, pp. 906–912, 2001.

[20] S. Zangooie, R. Jansson, and H. Arwin, "Ellipsometric characterization of anisotropic porous silicon Fabry-Perot filters and investigation of temperature effects on capillary condensation efficiency", *Journal of Applied Physics*, vol. 86, no. 2, pp. 850–858, 1999.

[21] C. Mazzoleni and L. Pavesi, "Application to optical components of dielectric porous silicon multilayers", *Applied Physics Letters*, vol. 67, no. 20, pp. 2983–2985, 1995.

[22] K. Kordás, S. Beke, A.E. Pap, A. Uusimäki, and S. Leppävuori, "Optical properties of porous silicon. Part II: Fabrication and investigation of multilayer structures", *Optical Materials*, vol. 25, pp. 257–260, 2004.

[23] M. Q. Brewster, *Thermal Radiative Transfer and Properties*, Wiley-Interscience, New York, NY, 1992.

[24] M. Braun and L. Pilon, "Effective optical properties of non-absorbing nanoporous thin-films", *Thin Solid Films*, vol. 496, pp. 505–514, 2006.

[25] J.C. Maxwell Garnett, "Colours in metal glasses and in metallic films", *Philosophical Transactions of the Royal Society of London, Series A*, vol. 203, pp. 385–420, 1904.

[26] D.A.G. Bruggeman, "Berechnung verschiedener physikalischer konstan ten von heterogenen substanzen", *Annals of Physics (Leipzig)*, vol. 24, pp. 636, 1935.

[27] J. A. del Rio, R. W. Zimmerman, and R. A. Dawe, "Formula for the conductivity of a two-component material based on the reciprocity theorem", *Solid State Communication*, vol. 106, no. 4, pp. 183, 1998.

[28] J. A. del Rio and S. Whitaker, "Maxwell's equations in two-phase systems I: Local electrodynamic equilibrium", *Transport in Porous Media*, vol. 39, pp. 159–186, 2000.

[29] J. A. del Rio and S. Whitaker, "Maxwell's equations in two-phase systems II: Two-equation model", *Transport in Porous Media*, vol. 39, pp. 259–287, 2000.

[30] M. Braun, "Effective optical properties of nanoporous thin-films", Master's thesis, Mechanical and Aerospace Engineering Department, University of California, Los Angeles, CA, 2004.

[31] K. Postava and T. Yamaguchi, "Optical functions of low-k materials for interlayer dielectrics", *Journal of Applied Physics*, vol. 89, no. 4, pp. 2189–2193, 2001.

[32] B. Sareni, L. Krähenbühl, and A. Beroual, "Effective dielectric constant of periodic composite materials", *Journal of Applied Physics*, vol. 80, no. 3, pp. 1688–1696, 1996.

[33] *FEMLAB 3 Electromagnetics Module User's Guide, Version 3.0*, Comsol AB, 2004.

[34] A.E. Pap, K. Kordás, J. Vähäkangas, A. Uusimäki, S. Leppävuori, L. Pilon, and S. Szatmári, "Optical properties of porous silicon. Part III: Comparison of experimental and theoretical results", *Optical Materials*, vol. 28, pp. 506–513, 2006.

[35] P. Ferrand and R. Romestain, "Optical losses in porous silicon waveguides in the near-infrared: Effects of scattering", *Applied Physics Letters*, vol. 77, pp. 3535–3537, 2000.

[36] G. Lerondel and R. Romestain, "Quantitative analysis of light scattering effects on porous silicon optical measurements", *Thin Solid Films*, vol. 297, pp. 114–117, 1997.

[37] L. S. Lasdon, A. D. Waren, A. Jain, and M. Ratner, "Design and testing of a generalized reduced gradient code for nonlinear programming", *ACM Transactions on Mathematical Software*, vol. 4, no. 1, pp. 34–49, 1978.

[38] M. F. Modest, *Radiative Heat Transfer*, McGraw-Hill, New York, NY, 2002.

[39] C.J. Brinker and C.W. Scherer, "Lorentz-Lorenz equation", in *Sol-Gel Science*, p. 803C. Academic Press, San Diego, 1990.

[40] G. Gülşen and M. Naci Inci, "Thermal optical properties of TiO_2 films", *Optical Materials*, vol. 18, pp. 373–381, 2000.

[41] C.F. Bohren and D.R. Huffman, *Absorption and Scattering of Light by Small Particles*, Wiley-Interscience, New York, 1983.

[42] R. Viskanta and M. P. Mengüç, "Radiative transfer in dispersed media", *Applied Mechanical Reviews*, vol. 42, no. 9, pp. 241–258, 1989.

Figure Captions

Figure 1. Schematic of the physical model and the corresponding finite element grid of the absorbing nanoporous thin film along with the boundary conditions.

Figure 2. Evolution of the through-plane effective index of refraction and absorption index of nanoporous SiO_2 thin films as a function of L/D for films with 19.63% porosity and pore diameters of 10 and 100 nm.

Figure 3. Root mean square δT as calculated according to Eq. (24) as a function of L/D.

Figure 4. Evolution of the through-plane effective index of refraction and absorption index as a function of porosity for nanoporous thin films with n_c=1.44, k_c=0.01, n_d=1.0, k_d=0.0, D=10 nm, and L/D=150.

Figure 5. Morphology of simulated nanoporous TiO_2 with cylindrical nanopores (left) or nanowires (right) for ϕ=0.2146.

Figure 6. Comparison of theoretical and numerical spectral transmittance and reflectance of nanoporous TiO_2 with cylindrical nanopores and nanowires of diameter D = 10 nm and porosity ϕ 0.2146 over the wavelength range between 400 and 900 nm and film thickness L = 150 D.

Figure 7. Comparison between the VAT model and numerically retrieved effective index of refraction and absorption index of dielectric medium ($m_c = 1.4 - i0.0$) with embedded metallic nanowires ($m_d = 1.66 - i1.96$) for various volume fractions and nanowire diameter.

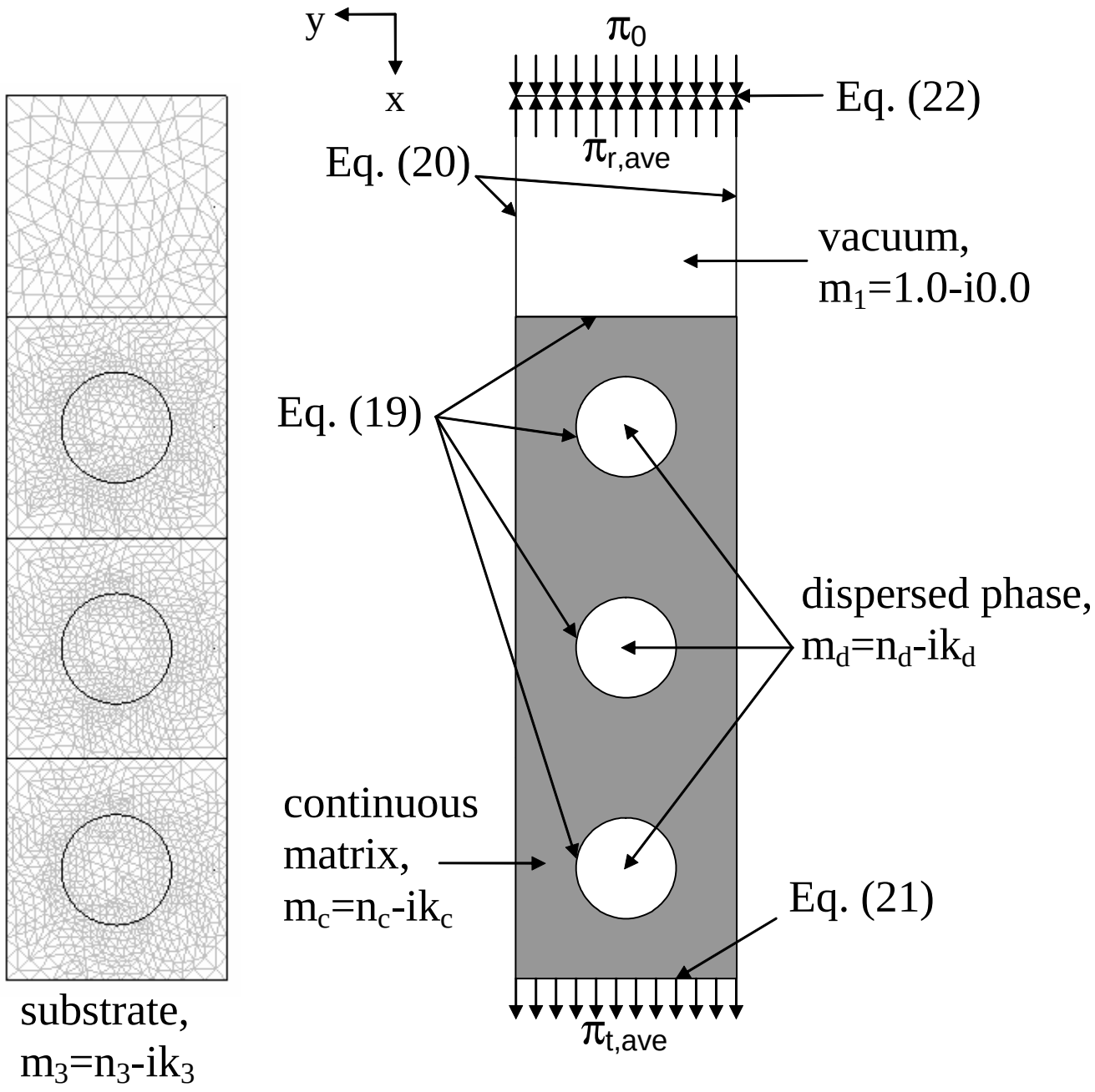

Figure 1: Schematic of the physical model and the corresponding finite element grid of the absorbing nanocomposite thin film along with the boundary conditions.

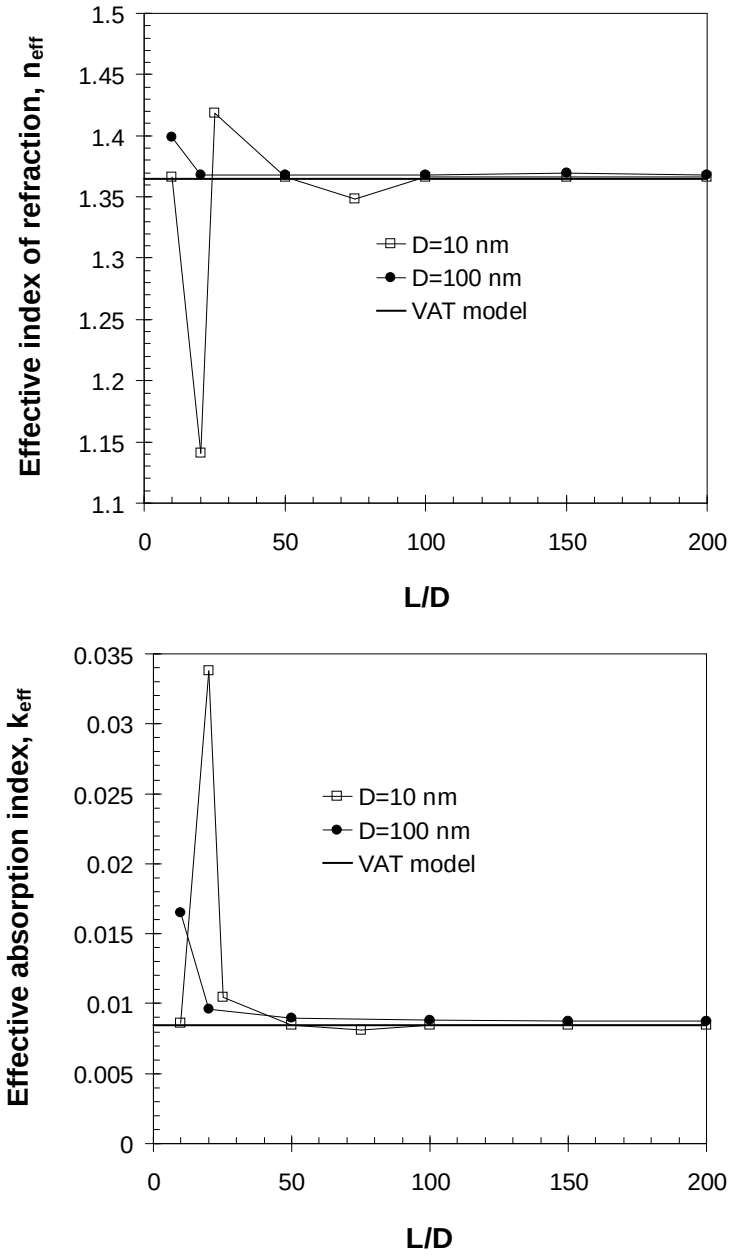

Figure 2: Evolution of the through-plane effective index of refraction and absorption index of nanoporous SiO_2 thin films as a function of L/D for films with 19.63% porosity and pore diameters of 10 and 100 nm.

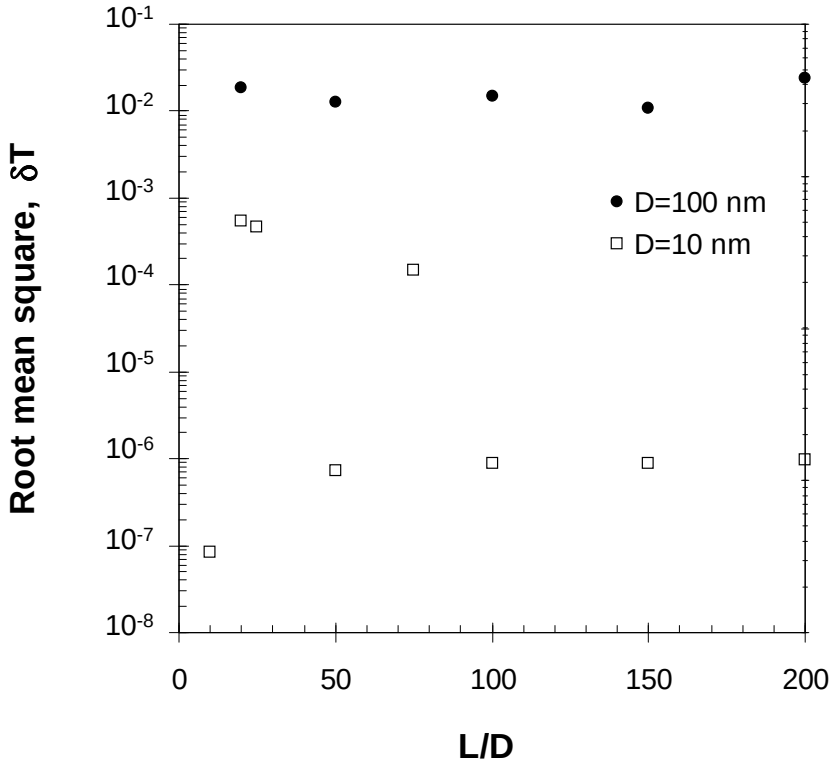

Figure 3: Root mean square δT as calculated according to Eq. (24) as a function of L/D for nanoporous SiO_2 thin films with ϕ=19.63% and pore diameter D equal to 10 and 100 nm.

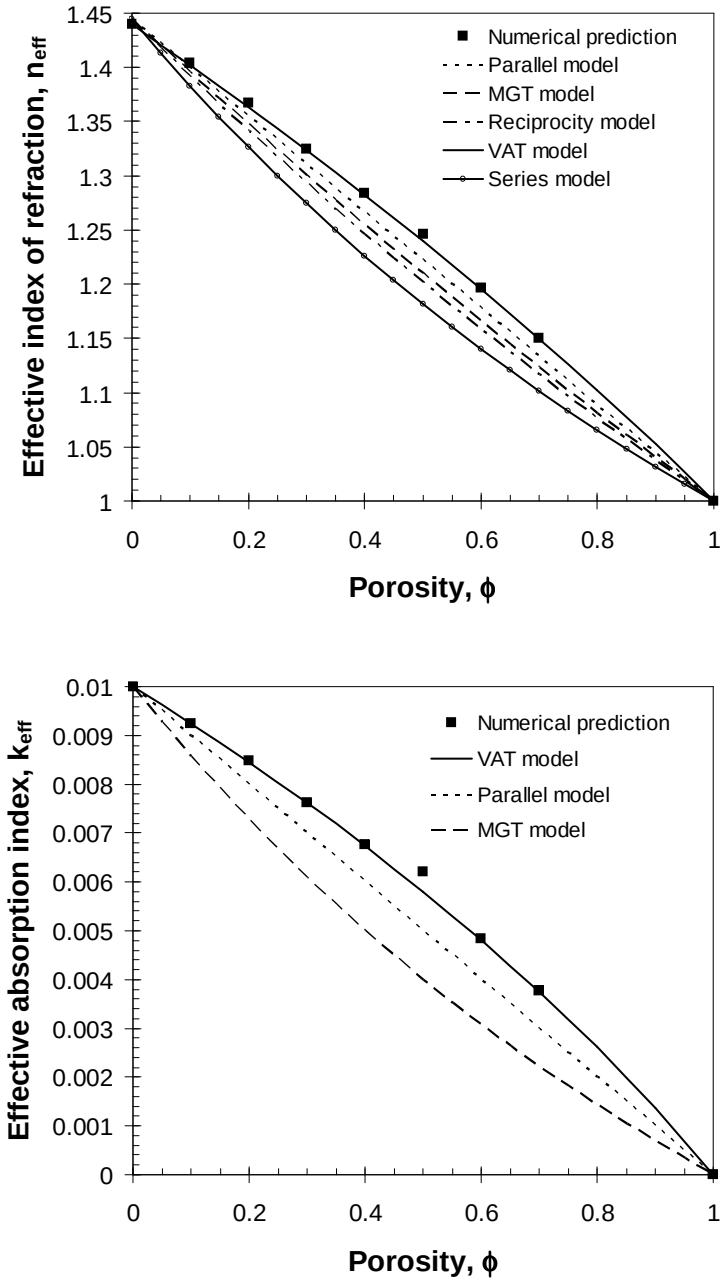

Figure 4: Evolution of effective index of refraction and absorption index as a function of porosity for nanoporous thin films with n_c=1.44, k_c=0.01, n_d=1.0, k_d=0.0, D=10 nm, and L/D=150.

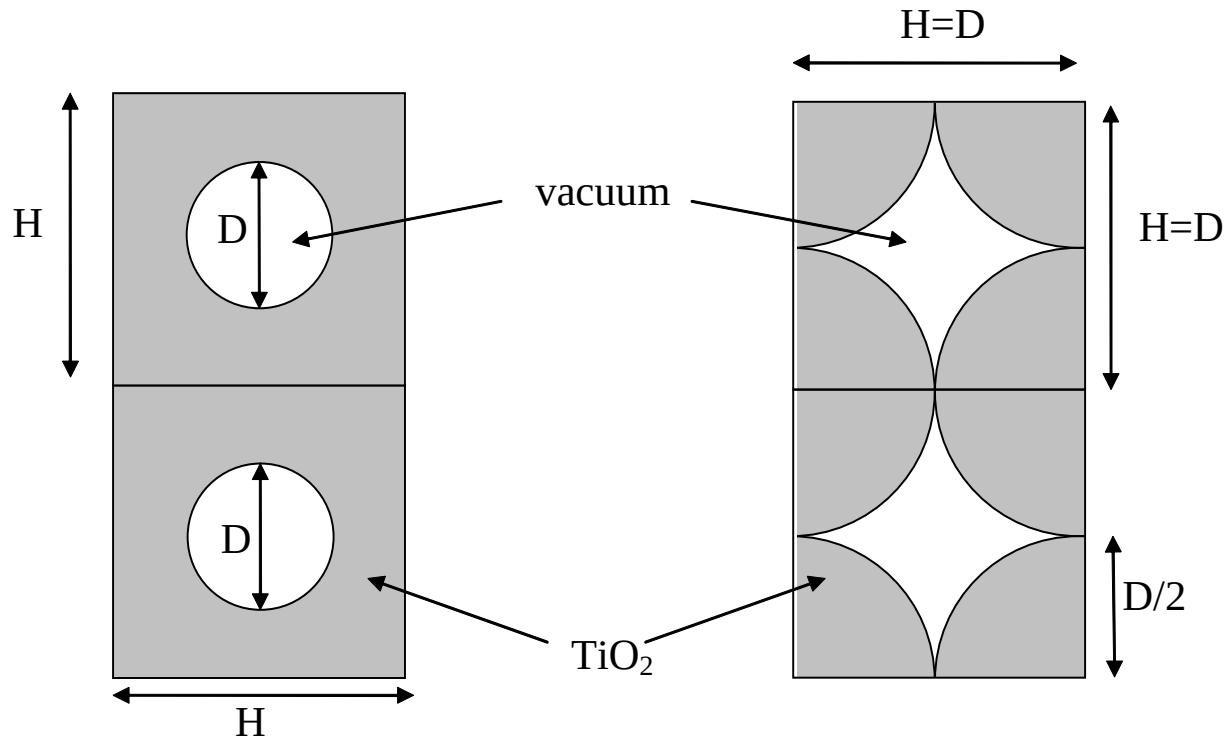

Figure 5: Morphology of simulated nanoporous TiO_2 with cylindrical nanopores (left) or nanowires (right) for ϕ=0.2146.

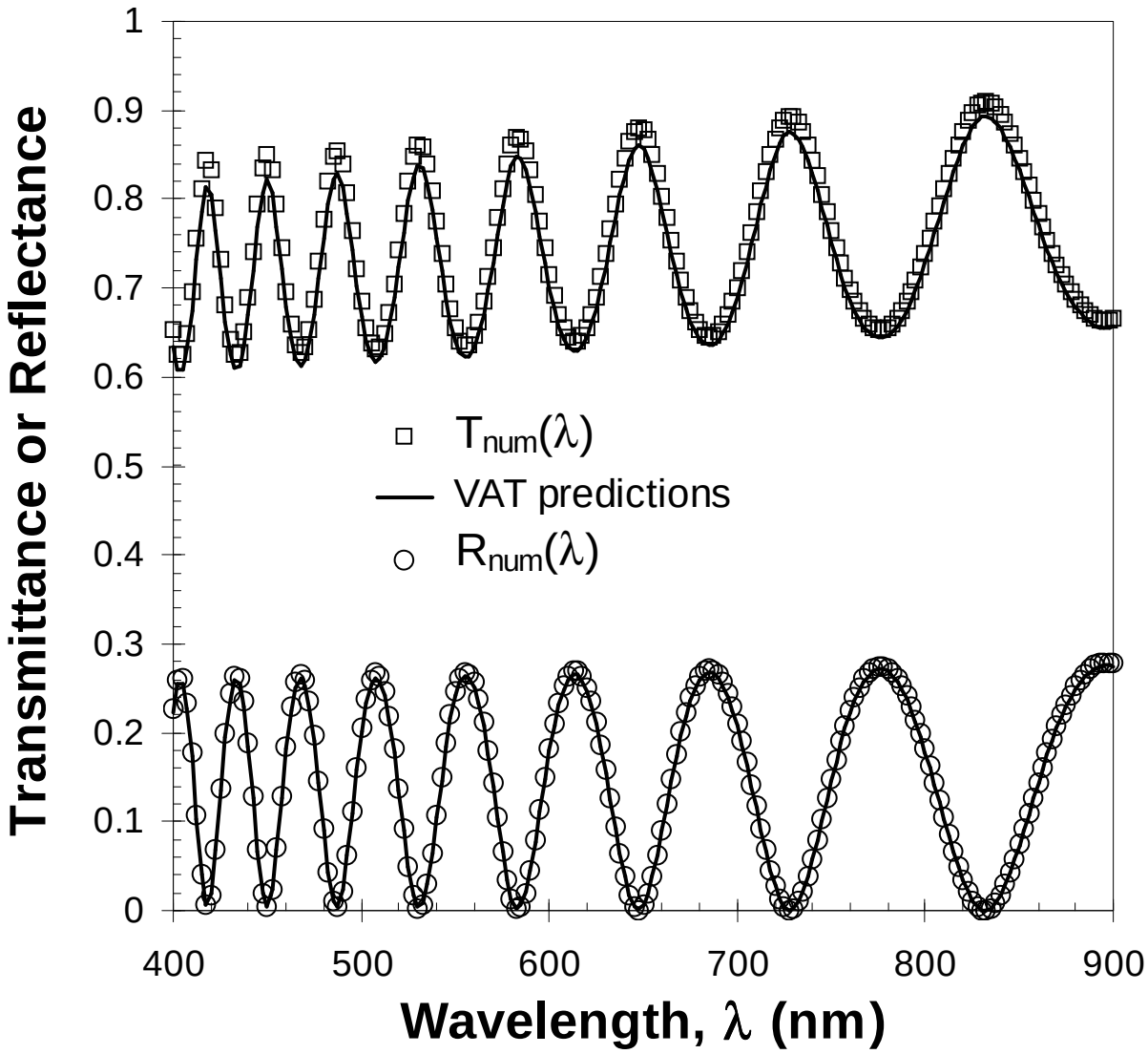

Figure 6: Comparison of theoretical and numerical spectral transmittance and reflectance of nanoporous TiO_2 with cylindrical nanopores and nanowires of diameter D = 10 nm and porosity ϕ 0.2146 over the wavelength range between 400 and 900 nm and film thickness L = 150 D.

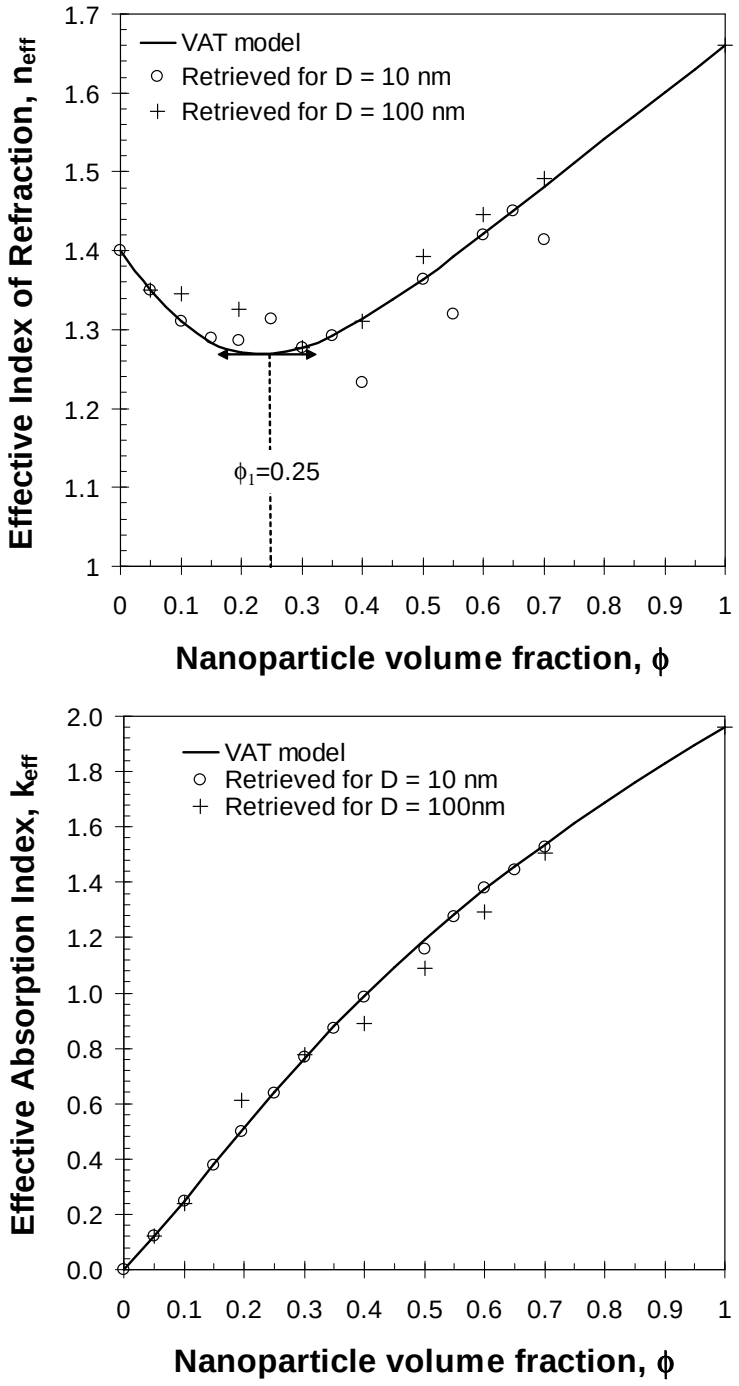

Figure 7: Comparison between the VAT model and numerically retrieved effective index of refraction and absorption index of dielectric medium ($m_c = 1.4 - i0.0$) with embedded metallic nanowires ($m_d = 1.66 - i1.96$) for various volume fractions and nanowire diameter.